Bidirectional FtsZ filament treadmilling promotes membrane constriction via torsional stress

Authors: Diego A. Ramirez-Diaz[1,2], Adrian Merino-Salomon[1], Michael Heymann[1] & Petra Schwille[1].

Affiliations:

[1].Department of Cellular and Molecular Biophysics, Max Planck Institute for Biochemistry, Martinsried, Germany

[2].Graduate School for Quantitative Biosciences (QBM), Ludwig-Maximillians-University, Munich, Germany

Abstract: FtsZ is a key component in bacterial cell division, being the primary protein of the presumably contractile Z ring. Reconstituted in vitro, it shows two distinctive features that could so far however not be mechanistically linked: self-organization into directionally treadmilling vortices on solid supported membranes, and shape deformation of flexible liposomes. In cells, circumferential treadmilling of FtsZ was shown to recruit septum-building enzymes, but an active force production remains elusive. To determine direct contributions of FtsZ to membrane constriction, we designed a novel in vitro assay based on soft lipid tubes pulled from FtsZ decorated giant lipid vesicles (GUVs) by optical tweezers. FtsZ actively transformed these tubes into spring-like structures, where GTPase activity promoted spring compression. Operating the optical tweezers in lateral vibration mode and assigning spring constants to FtsZ coated tubes, we found that that FtsZ indeed exerts pN forces upon GTP hydrolysis, through torsional stress induced by bidirectional treadmilling.

Main Text: In biology, fundamental mechanical processes, such as cell division, require an intricate space-time coordination of respective functional elements. However, how these elements, mostly proteins, can self-organize to exert forces driving large-scale transformations is poorly understood. In several organisms, ring-like cytoskeletal elements appear upon cytokinesis; for instance, the FtsZ-based contractile Z ring in bacteria. Ring-like FtsZ structures have previously been shown to deform liposome membranes (1,2). When reconstituted on flat membranes, FtsZ self-assembles into rotating-treadmilling vortices with conserved direction (3,4). *In vivo*, FtsZ shows circumferential but bi-directional treadmilling that is assumed to serve as a pacemaker guiding peptidoglycan synthesis (5,6). To date, however, there are conflicting views about whether GTP-consuming FtsZ treadmilling may also actively contribute to bacterial cytokinesis, as no physical force could so far be assigned to it. Therefore, using a novel optical tweezer-based approach by pulling soft lipid tubes from giant-unilamellar-vesicles GUVs, our aim is to quantitatively elucidate the physical principles underlying membrane-deformations induced by dynamic FtsZ rings on giant unilamellar vesicles (GUVs) and the scale of delivered forces.

Based on our recent study (3), we externally added FtsZ-YFP-mts to GUVs. Conditions to obtain ring-like structures were determined by tuning GTP and Mg^{+2} (Fig. 1A). Since no deformations were observed for tensed vesicles (Fig. 1A), we designed a two-side open chamber allowing for slow water evaporation to obtain deflated and deformable GUVs. After 30 minutes, we evidenced that rings were inducing cone structures emanating from the membrane, indicative of drilling-like inward forces (Fig. 1 B). Motivated by this, we designed PDMS microstructures mimicking such inward cones (Fig. 1C Fig 1SA). After coating these with lipid bilayer (SLB) and triggering protein polymerization, we observed individual filaments/bundles wrapping the cone in a dynamic fashion resembling a vortex (Fig. 1D) (Movie S1). We noticed that the dynamic vortices rotate clockwise and anticlockwise (Fig. 1E),

indicating that preferential directionality observed on flat SLBs is absent in spherical geometry. Rotational velocities were estimated around $43\,nm/s$, showing good agreement with our previous results on flat surfaces ($34\,nm/s$) (3). These results support the assumption of a helical architecture of FtsZ (*7*). Around the preferential diameter within the cone, a polar FtsZ helix will show clockwise treadmilling if it grows top-to-bottom and anticlockwise in reverse (bottom-to-top).

To quantitatively characterize the impact of FtsZ on soft tubular geometries, we developed a new method based on optical tweezers. Contrary to prior approaches using micropipettes (8), we pulled soft tubules from weakly surface-attached GUVs (Fig. 2SA) by moving the GUVs relative to an optically trapped bead. Tubes with mean diameter of ca. $0.5\,\mu m$ (Fig. 2SB) were now pulled from deflated GUVs decorated with ring-like FtsZ structures and inward-conical deformations (Movie S2). Once tubes were formed, protein filaments started entering and deforming the tube. After 175s, helical tube shapes were clearly observed (Fig. 2A), indicative of dynamic coiling (Movie S3). As more protein entered the tube and accumulated in the tip, the spring-like structure got compressed (Fig. 2A, 500s). These helical tube deformations can be rationalized by twisting of an elastic rod subjected to constant force (Fig. 2F). Similar to the experiment in Figure 1D, filaments grew towards (clockwise) and away from (counterclockwise) the tip of the tube. If filament growth imposes torsion, the counter-filament will generate torsion in the opposite direction. These two different torsional contributions result in the buckling of the lipid tube and the formation of a 3D helix (Fig. 2F). As previous studies have proposed, FtsZ torsion is here understood as an offset angle between two adjacent monomers (9) Further evidence for torsion is exhibited in plectonic/supercoiled regions (Fig. 1SE).

To investigate the role of GTP hydrolysis, we reconstituted FtsZ-YFP-mts*[T108A], a mutant with low GTPase activity (3). We observed that FtsZ-YFP-mts*[T108A] also self-assembled into ring-like structures (Fig. 1SB) that lacked dynamic treadmilling (3) yet still promoted inwards deformations (Fig. 1SC). Interestingly, the activity of FtsZ-YFP- mts*[T108A] on the tubes was much delayed (Fig. 2SC). Although helical deformations were also observed after 350s (Fig. 2C), their pitch remained considerably longer ($\lambda > 3\,\mu m$) also at long times (900s). In contrast, helices decorated with GTP-active FtsZ-YFP-mts (Fig. 2B) underwent compression to a pitch of $\lambda \sim 1.5\,\mu m$ after 300s. By plotting the arc-length of the spring against FtsZ density on the tube, we clearly observed a greater membrane-deforming activity for FtsZ-YFP-mts (Fig. 2D). Experiments shown in Fig. 2B-C correspond to similar tube diameters (d = 0.44 μm Fig. 2SB). We also tested whether compression could be biased by GUV deflation state and protein density. Although there was a mild correlation between pitch and diameter (Fig. 2SE), λ was consistently longer for FtsZ-YFP-mts*[T108A] (Fig. 2S E-F). Interestingly, both proteins show an initially larger pitch (Fig. 2E), suggesting that FtsZ binding to the tubes induces an intrinsic torsion, which is further enhanced by GTPase activity, compressing the helix.

To quantitatively characterize the mechanical properties of FtsZ-YFP-mts-induced spring-like structures, we implemented a novel approach based on the tube elastic response to a specific dynamic input. Using a piezoelectric stage, we induced a lateral oscillation of the GUV position to stretch the tube ($A = 3\,\mu m, f = 1\,Hz$) (Fig. 3A) and recorded forces by the tweezer (Movie S4). To model the system, we considered a spring constant contribution of the lipid k_l in a parallel configuration with FtsZ k_{FTSZ} (Fig. 3C). The force signal is depicted in Figure 3B, where the red line refers to the pure lipid tube and the green line to lipid-protein. From the measured amplitude, we could calculate a spring constant $k_l = 1.38 \pm 0.34\,pN/\mu m$. Next, we determined the spring constant (Fig. 3B) of helical FtsZ shaped tubes by subtracting the lipid contribution: $k_{FTSZ} = 1 \pm 0.29\,pN/\mu m$. Now we can estimate the required force to compress

the spring by GTPase activity. The torsional force contribution corresponding to the treadmilling activity can be determined as 1.5−2.5 pN.

Moreover, we could estimate FtsZ's Young's modulus E_{FTSZ} using k_{FTSZ} and k_l. The Young's modulus of a spring is related to the spring constant through $E = (k\, l_0)/S$, where l_0 is the spring initial length and S the cross-section. Since l_0/S was fairly constant, $E_{FTSZ} = (k_{FTSZ}/k_l)\, E_l$. The bending modulus of lipid bilayers can be estimated between $10 - 20 k_B T$ ($E_l = 11.5 - 23$MPa) (8, 10). Therefore, E_{FTSZ} can be estimated to $\sim 8.2 - 16.4\, MPa$. Consequently, FtsZ persistence length (lp) and bending rigidity (K) can also be inferred. Considering the bundling contribution in presence of Mg^{+2} (Supplementary text), we calculated a $lp \sim 0.7 - 1.4\, \mu m$ and a bending rigidity $K \sim 2.6 - 5.2\, x\, 10^{-27}\, Nm^2$ showing good agreement with a previous report (12) and the mean filament length of FtsZ (inside-rings) on SLBs (3). This persistence length was lower than for microtubules ($\sim mm$) and actin ($\sim 18\, \mu m$) (11,12) indicating that FtsZ-bundles are softer than other cytoskeleton proteins such as microtubules ($K \sim 10^{-23}$) or actin ($K \sim 10^{-26}$).

The helical membrane transformation caused by FtsZ filaments can be understood by assuming torque around the lipid tube. Darboux torques are tangential torques caused by a local mismatch between the plane defined by the filament curvature and the membrane attachment direction (13). To bind, filaments have to "stress" to align to the membrane, but this stress is released by inducing a "spin" on its internal frame, the Darboux frame (14). This twisting angle along the filament is key to produce torque. A molecular dynamics study showed that dynamin, an endocytic constriction helical protein, required twisting of the "adhesive-stripe" to achieve full membrane hemifusion (13). In the FtsZ case, molecular dynamics studies have predicted an angle of "twisting" between monomers (15, 16). Also, Fierling and coworkers have theoretically studied membrane deformations produced by filaments inducing Darboux torques (14). Strikingly, they found inward vortex-like deformations from flat surfaces and spring-like shapes when filaments wrapped around a tubular geometry (14). These predictions agree remarkably well with our observations. We can estimate the generated FtsZ-torque over one lp: $\tau/\varphi = (G \cdot J)/lp$ where G represents the shear modulus and $J = 2I$, the torsion constant. As a result, FtsZ could deliver torques around $1.2\, pN \cdot nm/rad$. As expected, this value is lower than ATP synthase FoF1 subunit ($31.2\, pN \cdot nm/rad$) (17) or dynamin ($\sim 500\, pN \cdot nm/rad$) (18).

So far, we had investigated an inverse geometry, i.e., FtsZ added from the outside, as compared to the physiological case. Now we also reconstituted FtsZ-YFP-mts and FtsZ-YFP-mts*[T108A] inside GUVs (Fig. 4A). Conditions to obtain rings- like-structures (Fig. 4 B) or filaments wrapping the vesicle (Fig. 1SD) were again found by tuning GTP and Mg^{+2}. Interestingly, the diameters of FtsZ-YFP-mts*[T108A] rings were significantly larger ($0.89\, \mu m$) than FtsZ-YFP-mts ($0.44\, \mu m$) (Fig.4D). This difference was not observed in the case of SLBs (3) indicating that either the surface-to-volume ratio or a softer lipid surface ruled the assembly in steady state. In addition, the wide size distribution in the low GTPase mutant case (Fig. 4D) implied that polymers were flexible to accommodate a larger variety of curvatures. Strikingly, both FtsZ mutants could create outwards deformations emerging from rings (Fig. 4E). But only in the case of FtsZ-YFP-mts, there was clear evidence of constricting rings (Fig. 4E) similar to previous reports (1). Based on Fig. 1, we hypothesize that FtsZ torsion could create outwards out-of-plane forces (Fig. 4F). However, FtsZ filaments only exhibiting static (structural) torsion were unable to stabilize smaller diameters. In contrast, dynamic twisting upon GTP-hydrolysis drives constriction and clustering (Fig. 4G). Upon GTP, FtsZ filaments support smaller diameters. FtsZ constriction and neck formation thus represents an

equivalent situation of helix compression when protein was external to the tube, suggesting a similar force required for constriction from relaxed to compressed state of 1.5−2.5 pN.

Altogether, our experiments provide clear evidence that FtsZ induces two kinds of mechanical deformations to membranes. Static (structural) FtsZ torsion rules the assembly of rings on flat surfaces (3) and induces inwards/outwards deformations. Importantly, circumferential treadmilling powered by GTP hydrolysis induces additional torque-twist, leading to and supporting further membrane constriction. Regardless whether protein was externally added or encapsulated, cylindrical geometry allowed clockwise and anti-clockwise treadmilling (Fig. 4E). Together they induce helical transformation of the membrane tube and a super-constricted state of filaments, imposing a mechanical strain that promotes breakage (Fig. 4G). This establishes an interesting similarity between FtsZ and dynamin, in which GTP hydrolysis also triggers a super-constricted state, favoring fragmentation and clustering (19,20). We conclude that these torques represent a robust constriction mechanism for cylindrically shaped membranes. Although the here reported forces may not suffice for bacterial cytokinesis (~ 2 pN), they could induce neck formation if membrane tension is lowered; for instance, through the incorporation of de novo synthesized lipids.

References:

1. T M. Osawa, D. E. Anderson, H. P. Erickson, Reconstitution of Contractile FtsZ Rings in Liposomes. *Science*. **320**, 792–794 (2008).
2. M. Osawa, H. P. Erickson, Liposome division by a simple bacterial division machinery. *PNAS*. **110**, 11000–11004 (2013).
3. D. A. Ramirez-Diaz *et al.*, Treadmilling analysis reveals new insights into dynamic FtsZ ring architecture. *PLOS Biology*. **16**, e2004845 (2018).
4. M. Loose, T. J. Mitchison, The bacterial cell division proteins FtsA and FtsZ self-organize into dynamic cytoskeletal patterns. *Nat Cell Biol*. **16**, 38–46 (2014).
5. A. W. Bisson-Filho *et al.*, Treadmilling by FtsZ filaments drives peptidoglycan synthesis and bacterial cell division. *Science*. **355**, 739–743 (2017).
6. X. Yang *et al.*, GTPase activity–coupled treadmilling of the bacterial tubulin FtsZ organizes septal cell wall synthesis. *Science*. **355**, 744–747 (2017).
7. P. Szwedziak, Q. Wang, T. A. M. Bharat, M. Tsim, J. Löwe, Architecture of the ring formed by the tubulin homologue FtsZ in bacterial cell division. *eLife*. **3**, e04601 (2015).
8. A. Roux *et al.*, Membrane curvature controls dynamin polymerization. *PNAS*. **107**, 4141–4146 (2010).
9. P. G. de P. Salas *et al.*, Torsion and curvature of FtsZ filaments. *Soft Matter*. **10**, 1977–1986 (2014).
10. L. Picas, F. Rico, S. Scheuring, Direct Measurement of the Mechanical Properties of Lipid Phases in Supported Bilayers. *Biophysical Journal*. **102**, L01–L03 (2012).
11. F. Gittes, B. Mickey, J. Nettleton, J. Howard, Flexural rigidity of microtubules and actin filaments measured from thermal fluctuations in shape. *The Journal of Cell Biology*. **120**, 923–934 (1993).
12. J. van Mameren, K. C. Vermeulen, F. Gittes, C. F. Schmidt, Leveraging Single Protein Polymers To Measure Flexural Rigidity. *J. Phys. Chem. B*. **113**, 3837–3844 (2009).
13. D. J. Turner *et al.*, The Mechanics of FtsZ Fibers. *Biophysical Journal*. **102**, 731–738 (2012).
14. M. Pannuzzo, Z. A. McDargh, M. Deserno, The role of scaffold reshaping and disassembly in dynamin driven membrane fission. *eLife*. **7**, e39441 (2018).

15. J. Fierling, A. Johner, I. M. Kulić, H. Mohrbach, M. M. Müller, How bio-filaments twist membranes. *Soft Matter*. **12**, 5747–5757 (2016).
16. J. Hsin, A. Gopinathan, K. C. Huang, Nucleotide-dependent conformations of FtsZ dimersand force generation observed through molecular dynamics simulations. *PNAS*. **109**, 9432–9437 (2012).
17. S. Toyabe, T. Watanabe-Nakayama, T. Okamoto, S. Kudo, E. Muneyuki, Thermodynamic efficiency and mechanochemical coupling of F1-ATPase. *PNAS*. **108**, 17951–17956 (2011).
18. S. Morlot *et al.*, Membrane Shape at the Edge of the Dynamin Helix Sets Location and Duration of the Fission Reaction. *Cell*. **151**, 619–629 (2012).
19. A. Colom, L. Redondo-Morata, N. Chiaruttini, A. Roux, S. Scheuring, Dynamic remodeling of the dynamin helix during membrane constriction. *PNAS*. **114**, 5449–5454 (2017).
20. T. Takeda *et al.*, Dynamic clustering of dynamin-amphiphysin helices regulates membrane constriction and fission coupled with GTP hydrolysis. *eLife*. **7**, e30246 (2018).

Acknowledgments: We acknowledge Sven Vogel, German Rivas and Allen Lui for very useful input. Funding through MaxSynBio consortium (Federal Ministry of Education and Research of Germany and the Max Planck Society) grant number 031A359A. The authors have declared that no competing interests exist. All data is available in the main text or the supplementary materials.

Figure 1.

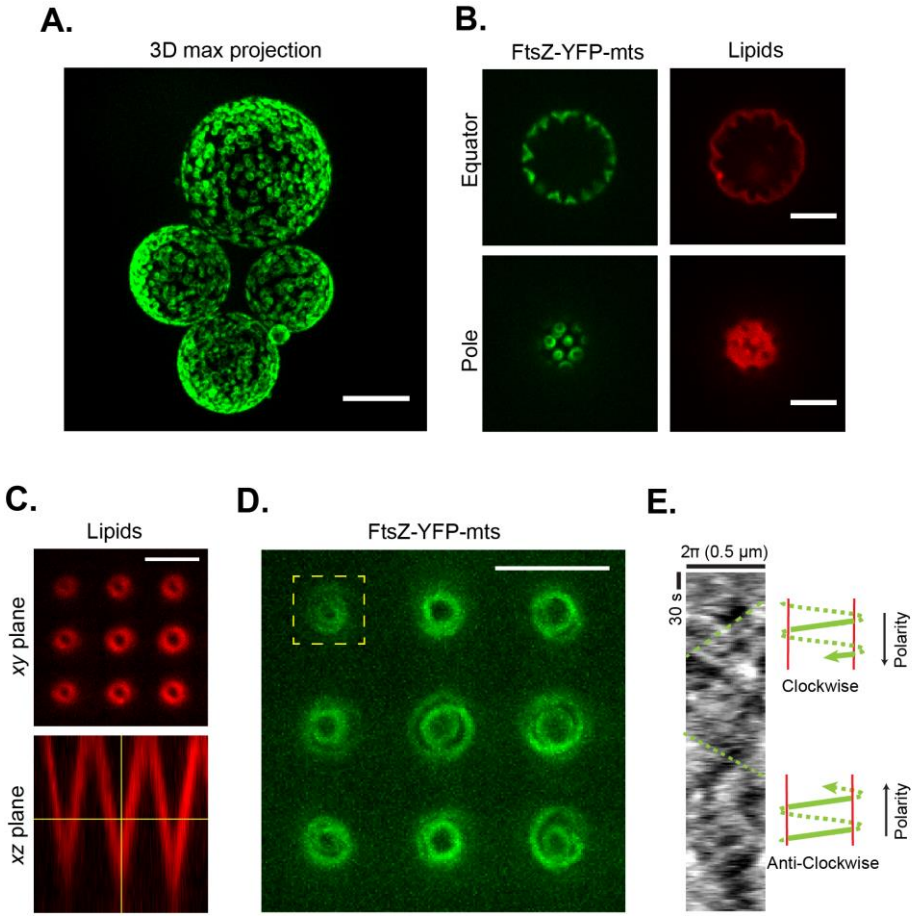

A) FtsZ-YFP-mts ring structures externally decorating GUVs (scale bar=10um). **B)** After GUV deflation, inwards conical deformations emerged from FtsZ rings. **C)** Inspired by deformations in (B), we designed a PDMS microstructure with inwards-conical geometry covered with a SLB. The imaging plane was chosen to have a cross-section of ~1 um diameter. **D)** Inside cones, FtsZ-YFP-mts self-assembled into dynamic vortices (Movie S1). **E)** Kymograph showed negative and positive slopes indicating the presence of clockwise and anticlockwise directions (Scale bar = 5 um).

Figure 2.

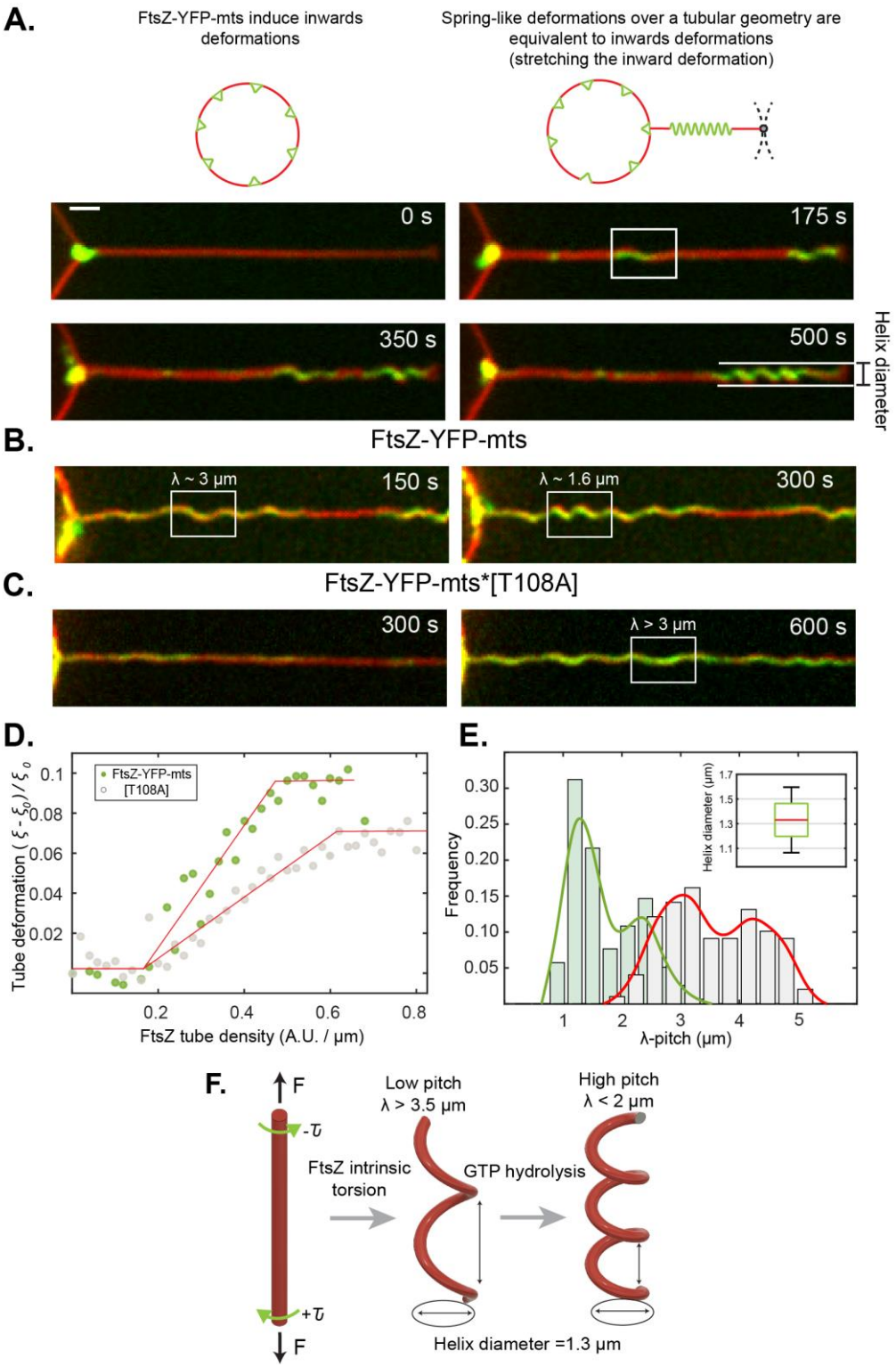

To understand inwards deformations, we stretched the cone structures in a tubular geometry. FtsZ-YFP-mts caused spring-like deformations exhibiting coiling and winding (Movie S3). Same diameter tubes decorated with **B)** FtsZ-YFP-mts **C)** and FtsZ-YFP-mts*[T108A]. Both proteins generated helical deformations with the difference that GTPase activity (green dots) induce compression (λ ~ 1.6 um) of initially longer pitch (λ > 3 um). **D)** GTPase activity caused greater deformation evidenced by tube deformation as function of FtsZ tube density **E)** We observed two clear pitch states for FtsZ-YFP-mts and FtsZ-YFP-mts*[T108A] (gray bars/red

line) with a clear dominance of longer pitch for the mutant without GTPase activity. **F)** Helical deformations can be understood by twisting an elastic rod subjected to constant force. We postulate that FtsZ has an intrinsic torsion than is enhanced by GTPase activity, driving further compression. Intrinsic FtsZ torsion rules low-pitch transformations ($\lambda > 3$ um) while GTP enhances further torsion causing higher pitch states ($\lambda < 2$ um).

Figure 3.

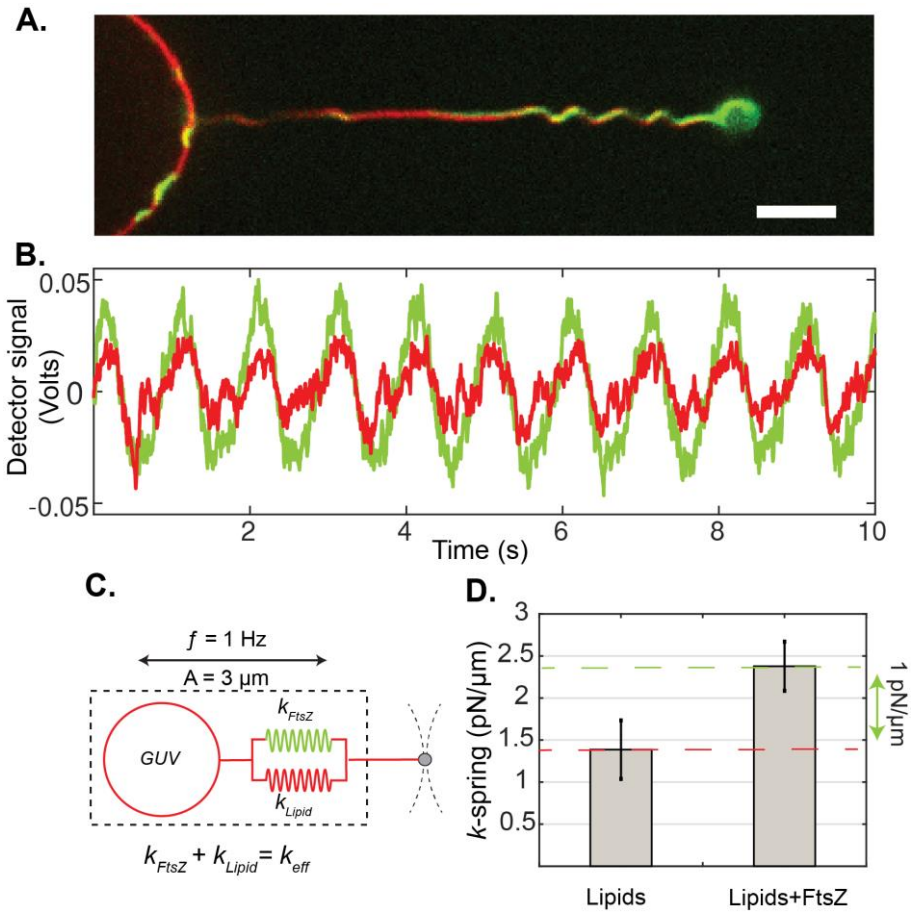

A) Spring-like structures were mechanically assessed by **C)** forcing the tube length to oscillate with an amplitude of 3 μm and a frequency of $1 Hz$. For modelling, we considered a spring-constant contribution of the lipid in a parallel configuration with FtsZ contribution. **B)** To measure forces, we tracked bead-displacement as response of the dynamic input. Red line: lipid signal and green line: FtsZ. **D)** By calculating the amplitude, we measured the FtsZ spring constant k=1±0.29 pN/µm.

Figure 4.

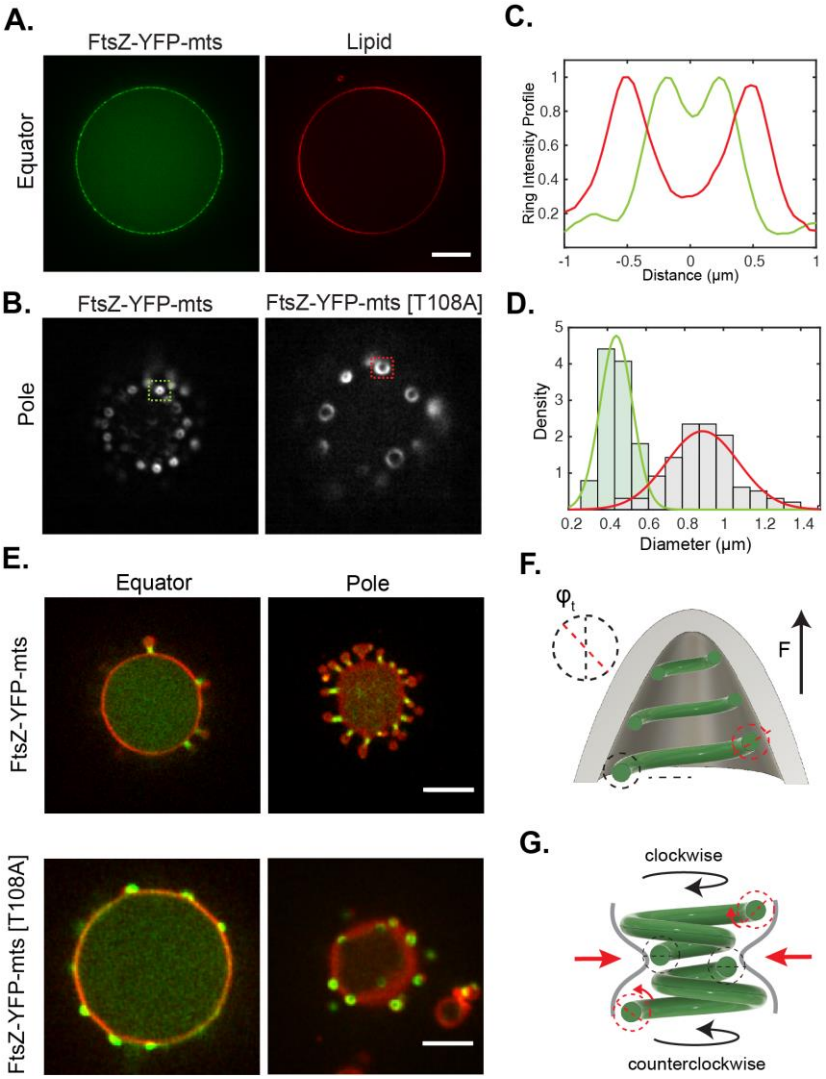

A) FtsZ-YFP-mts and FtsZ-YFP-mts*[T108A] rings inside GUVs. **B)** Imaging of rings, at GUVs bottom, using TIRF microscopy. **C)** Intensity profile of structures indicated in (B) showed that FtsZ-YFP-mts (green line) rings exhibit smaller diameter than FtsZ-YFP-mts*[T108A] (red line). **D)** Size distribution of FtsZ-YFP-mts*[T108A] (gray bars and red line) and FtsZ-YFP-mts showed a drastic reduction in ring diameter due to GTP hydrolysis. **E)** After deflation, both mutants drove outwards deformations with the difference that GTPase activity promotes constriction and neck formation. **F)** We suggest that intrinsic torsion can create out-of-plane forces; however, **G)** GTP hydrolysis triggered a super-constricted state favoring higher curvatures.